Electronic Supplementary Material (ESI) for Journal of Materials Chemistry A.

Supplementary Information

Effect of structure on oxygen diffusivity in layered oxides: A combined theoretical and experimental study

ChangSub Kim[a,b,†], Kyoung-Won Park[c, †], Dmitri Kalaev[a], Clement Nicollet[a,d], Harry L. Tuller[a,*]

[a] Department of Materials Science and Engineering, Massachusetts Institute of Technology, Cambridge, MA 02139, USA

[c] Materials Architecturing Research Center, Korea Institute of Science and Technology, 5 Hwarang-ro 14-gil Seongbuk-gu, Seoul 02792, Republic of Korea

Corresponding author

* E-mail: tuller@mit.edu

Present Addresses

[b] Jet Propulsion Laboratory, California Institute of Technology, Pasadena, California 91109, United States

[d] Université de Nantes, CNRS, Institut des Matériaux Jean Rouxel, IMN, Nantes, France

†: equally contributed

1. Crystal structures of A_2CuO_4

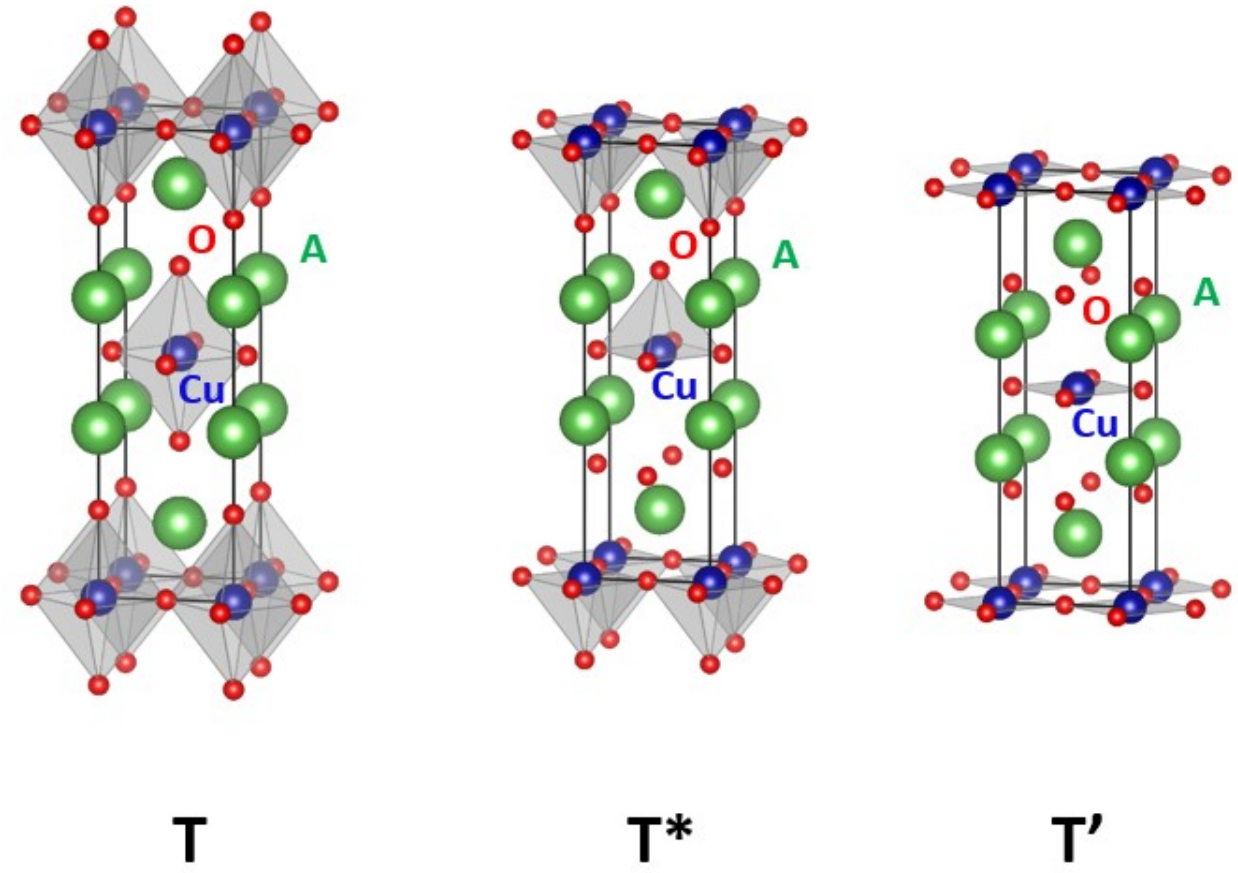

Figure S1. T, T*, and T’ structures of A_2CuO_4 layered cuprates. The key difference among the three structures is Cu-O coordination: octahedral (T), pyramidal (T*), and square-planar (T’).

2. Oxygen isotope exchange apparatus

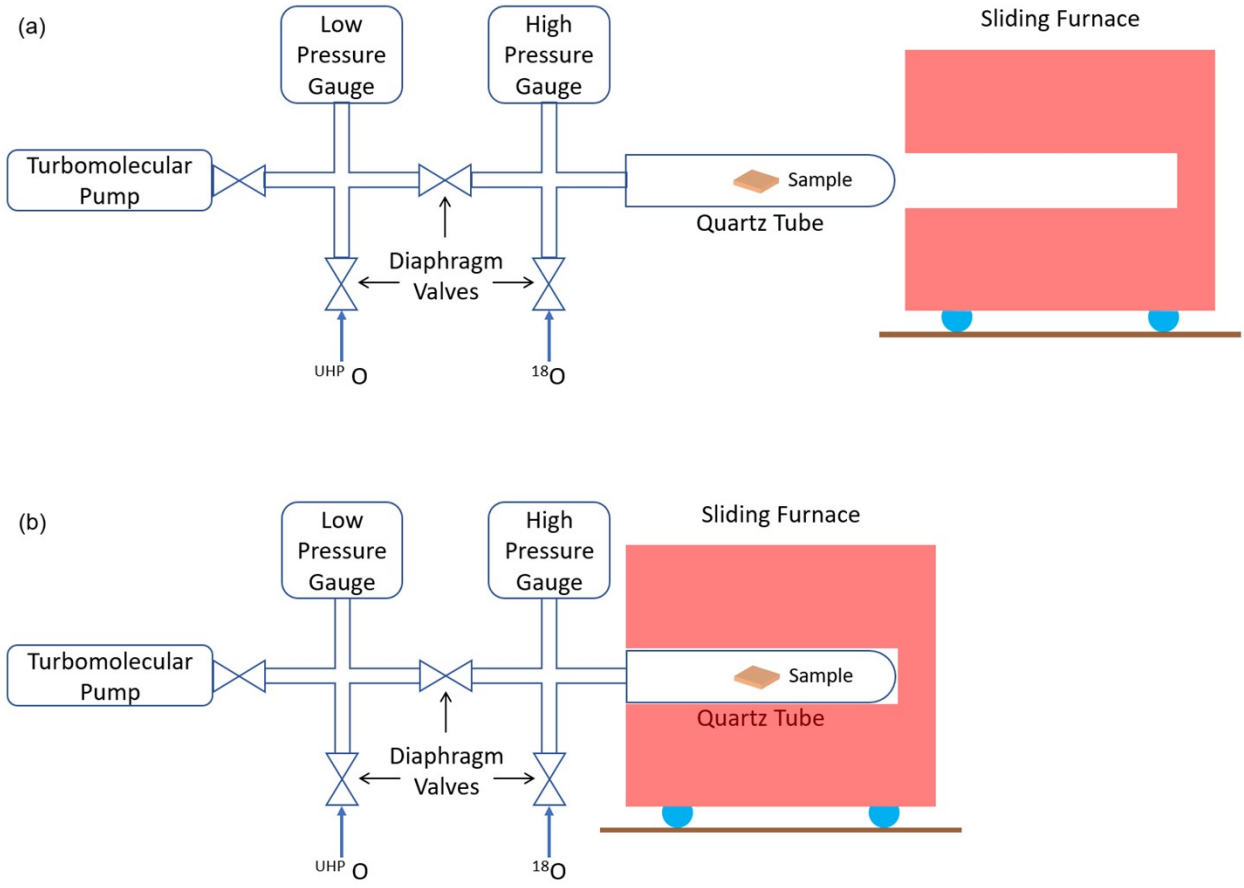

Figure S2. Schematic illustrations of the oxygen isotope exchange apparatus. **(a)** First, the sample is placed in the quartz tube then pumped down to ultra high vacuum (UHV) by a turbomolecular pump. The tube is filled with ultra high purity oxygen to a desired pressure, then **(b)** the furnace slides to enclose the tube and bring the specimen rapidly to elevated temperatures. After a period of time (at least ten times the isotope annealing time in the second step), the furnace slides back (a) and the quartz tube is quenched to room temperature by fan air. The process is repeated, but this time filled with ^{18}O.

3. Strain in LCO thin films

We summarized the lattice constants of T and T'-La_2CuO_4 in the table below. Both structures have tetragonal structures (space group = I4/mmm), but with different lattice constants[1,2]. The a=b and c lattices extracted from STEM-HAADF and -BF images in Figure 3 are 3.79±0.01 and 13.03±0.03 Å for T-LCO, and 4.003±0.03 Å and 12.35±0.05 Å for T'-LCO, respectively, in reasonable agreement with the ones in the literatures.

Structure	***a*=*b* (Å)**	***c* (Å)**
T-La_2CuO_4	3.803	13.15
T'-La_2CuO_4	4.005	12.55

According to the previous experimental results[1,2], increasing x in $La_{2-x}Ce_xCuO_4$ does not change *a*=*b*, but decreases the lattice parameter along the *c*-axis. The $La_{1.85}Ce_{0.15}CuO_4$ (LCCO15) seed layer has lattice parameters *a*=*b* = 4.01~4.02 Å and *c* = 12.425 Å, and thus T'-LCO grown on top experiences negligible lattice mismatch and strain. The $LaAlO_3$ substrate (LAO, space group = $Pm\bar{3}m$) has lattice constants *a*=*b*=*c* = 3.787 Å at room temperature. Therefore, T-LCO grows epitaxially with c-axis perpendicular to the surface of LAO without rotation as observed with HRXRD analysis and STEM images, and the strain experienced by T-LCO is -0.421% (compressive strain). Since the thermal expansion coefficients of LCO and LAO are almost identical (~10×10^{-6}/K), it is safe to assume that there is no change in strain experienced by the film over the temperature range of the experiment (500~600 ℃). STEM-HAADF and -BF images of T-LCO thin film/LAO substrate in Figure S3 show no structural defects such as edge dislocations along the interface. This confirms that there is no significant strain acting on the T-LCO film.

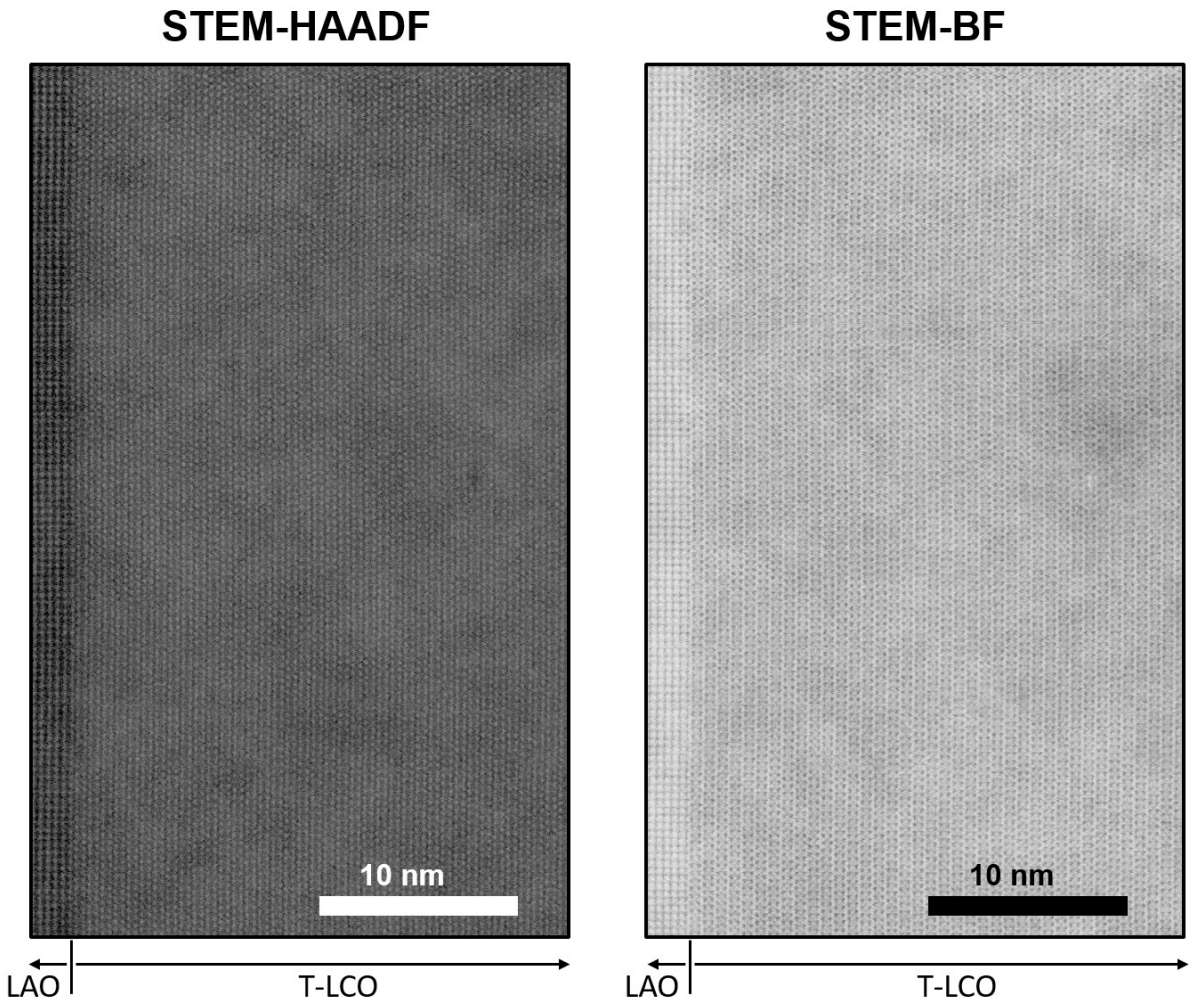

Figure S3. STEM-HAADF and –BF images of T-LCO thin film/LAO substrate.

As an example, defect formation energies for T-LCO are calculated with and without the compressive strain of 0.421% and compared in Figure S4. The defect formation energies are nearly identical for all types of oxygen defects, as expected from such a small strain.

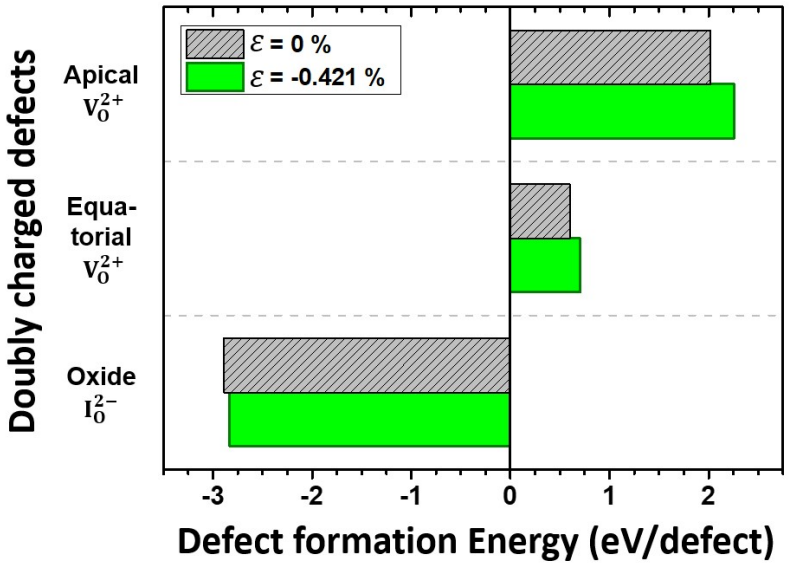

Figure S4. DFT calculated defect formation energy of doubly charged defects with and without strain (ε = 0 and -0.421 %).

4. Selection of U_{eff} value

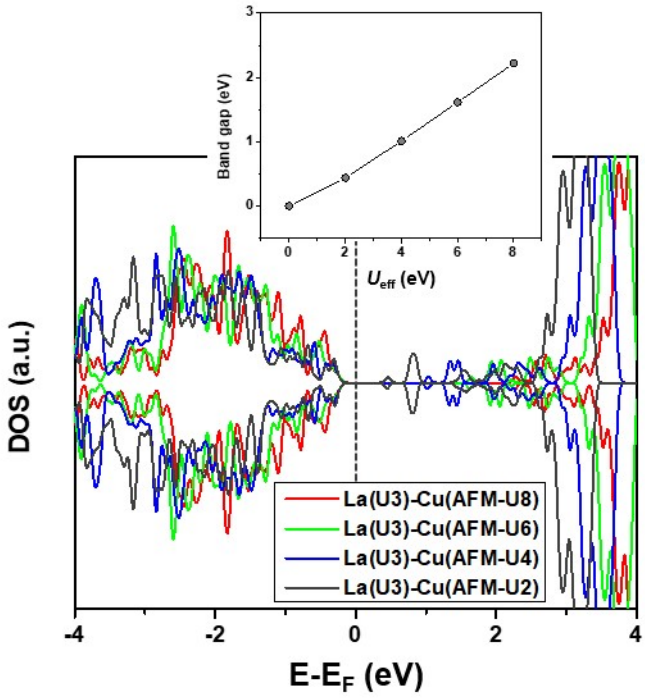

Figure S5. Total density of states (DOS) of bulk T-La_2CuO_4 of antiferromagnetic type-II (AFM-II), computed with various U_{eff} for Cu atoms and fixed U_{eff}= 3 eV for La atoms. E_F is the Fermi energy. Inset: band gap of bulk T-La_2CuO_4, with respect to the U_{eff} applied to Cu atoms.

5. Energy correction in defect formation energy calculation

As explained in Method 3.2 section in the main text, defect formation energies of charged defects were calculated using equation (1)[3,4] as defined below

$$E_f^{defect} = E_{tot}^{defect:q} - E_{tot}^{perfect} + \sum n_O \mu_O + q(E_F + E_{VBM}^{perfect} + \Delta V_{avg}), \quad (1)$$

Among the terms in eq. (1), the last two terms $q(E_{VBM}^{perfect} + \Delta V_{avg})$ are the same as E_{corr} which is a correction term that accounts for finite k-point sampling in the case of shallow impurities or for elastic and/or electrostatic interactions between supercells, introduced in refs[3,5]. $E_{VBM}^{perfect}$ is the VBM (valence band minimum) of the perfect supercell, which is obtained by $E_{tot}^{perfect} - E_{tot}^{perfect,+1}$, where $E_{tot}^{perfect,+1}$ is the total energy of the +1 charged perfect supercell. We obtained $E_{tot}^{perfect}$ and $E_{tot}^{perfect,+1}$ from DFT relaxations with neutral and +1 charge in the perfect LCO supercells. ΔV_{avg} is the difference between average potentials (V_{avg}) far from the defect relative to the perfect supercell, *i.e.*, $\Delta V_{avg} = V_{avg}^{defect:q} - V_{avg}^{perfect}$, in which $V_{avg}^{defect:q}$ and $V_{avg}^{perfect}$ are the average potentials of the defective and perfect supercells, respectively. For the calculations of $V_{avg}^{defect:q}$ and $V_{avg}^{perfect}$ terms, we obtained planar-averaged Hartree potentials of LCO supercells along *c*-axis, with and without defects, as shown in Figure S6 (a). Depending on the presence of the defect, potentials fluctuate around the defects compared to that of the perfect supercell. For the macro-averaged potential profiles, we conducted Baldereschi averaging[6] three times – examples shown in Figs. S6 (b) and (c). For the perfect supercell (Figure S6(b)), as macro-averaging is repeated, we can see that the profile is coarse. After averaging three times, the profile (orange line) becomes almost flat at around the potential = 0 V (green dotted line), because there is no large change in the macro-averaged-potential in the perfect supercell. In a defective supercell (for example, a supercell containing an apical V_O^{2+} as shown in Figure S6 (c)), the average potential far from the defect (L/2 away from the defect position (red triangle in Figure S6 (c))) still shows a plateau as observed in the perfect supercell. We read the macro-averaged potential at the red triangle as $V_{avg}^{perfect}$, the macro-averaged potential at the defect (blue triangle) as $V_{avg}^{defect:q}$, and then calculated ΔV_{avg} value.

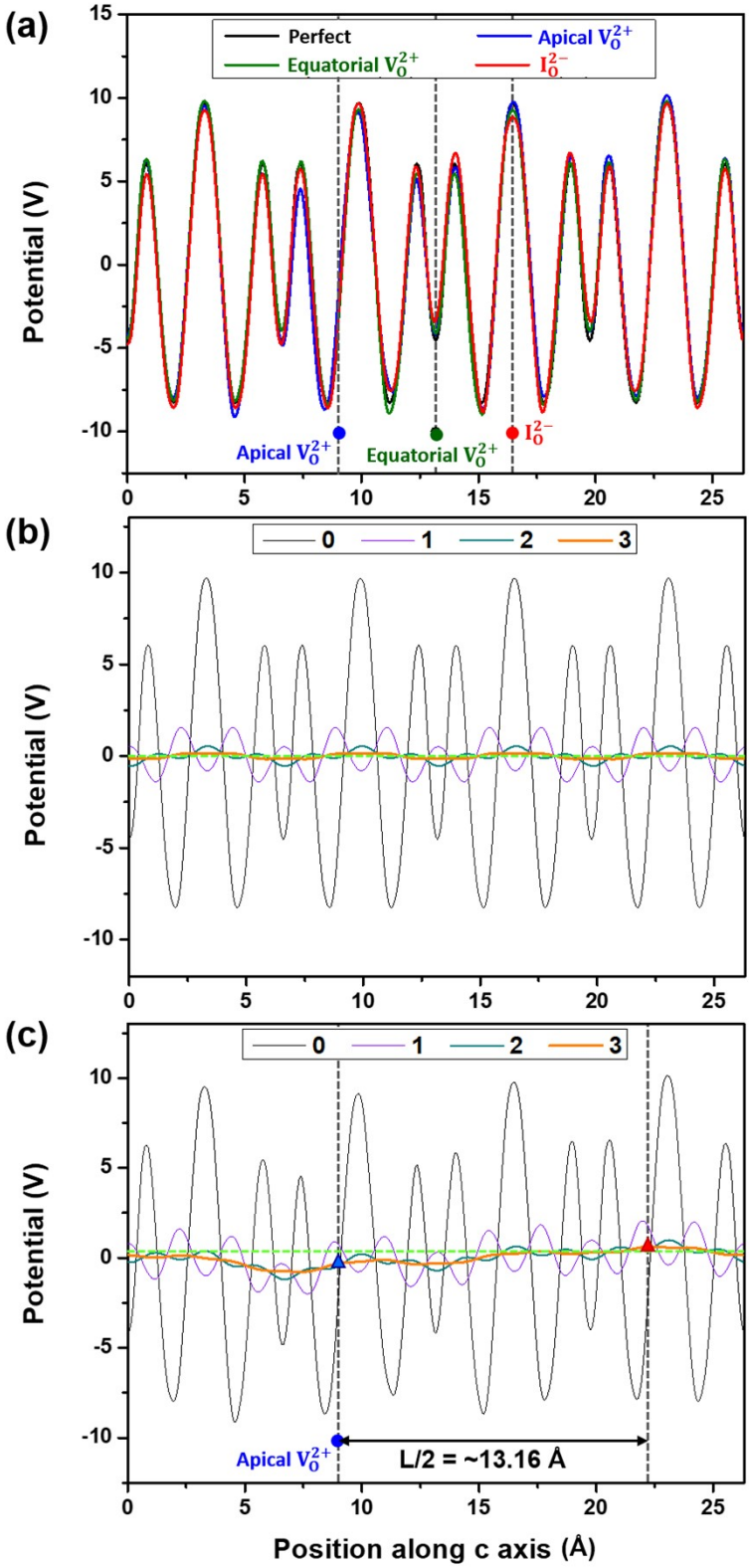

Figure S6. (a) Planar-averaged potential profiles of perfect supercell and supercells containing oxygen defects (apical oxygen vacancy V^{2+}_{O}, equatorial oxygen vacancy V^{2+}_{O}, oxide interstitial I^{2-}_{O}). Blue, green,

red dots indicate the location of oxygen defects in the supercells, respectively. **(b)** Macro-averaged potential profiles of perfect supercell along *c*-axis. Numbers in the legend (0, 1, 2 and 3) denote the number of averaging time. The horizontal green dotted line denote potential = 0 V. **(c)** Macro-averaged potential profiles of supercell with apical V_O^{2+}, along *c*-axis. Blue and red triangles denote the average potential at the defective supercell ($V_{avg}^{defect:q}$) and far from the defect, that is, at the perfect supercell ($V_{avg}^{perfect}$). L indicates the length of the supercell along *c*-axis.

This calculation was done before the calculation of defect formation energy of charged defects[7] (in large CeO_2 supercell of 96 atoms). The calculated formation energy of doubly charged defects in our previous study showed similar value to other researchers' calculation done with correction term E_{corr} [8]. Furthermore, the formation energy of doubly charged defect calculated with the same method as ref[7] describes the formation of the defect observed in the experimental evidence. Moreoever, the result from the study well predicts the dominant formation of oxygen interstitials in T-La_2CuO_4, in accordance with previous results from multiple computation/experiments[9–13]. Therefore, we verify that the defect formation energy calculation method used in this study is valid.

There is no universal correction method for the energy correction and the correction is often required in small supercells which are prone to large errors. Unrealistically large defect concentrations in small supercells result in artificial interactions between defects that cannot be neglected. The supercell used in this study is composed of 112 atoms and the concentration of oxygen defects in this study is $\delta = 0.016 \sim 0.032$ in $La_2CuO_{4\pm\delta}$, which is considerably smaller than typical concentrations of $\delta = 0.06 - 0.25$ in smaller supercells. Since macroscopic bulk behavior for electrostatic screening or elasticity is typically recovered to within 0.01 eV at a distance of only 5 – 10 Å from the defect center[5], our supercell (24 – 26.3 Å along *c*-axis) can minimize the error coming from short-range interactions. The concentration of oxygen defects chosen in this study has also proved to be within a similar range as experimentally measured values $\delta = 0.01 - 0.02$ [14,15]. We believe that our supercell is large enough to describe the defects in the experimentally prepared La_2CuO_4 specimens.

6. Diffusion energy barrier calculations

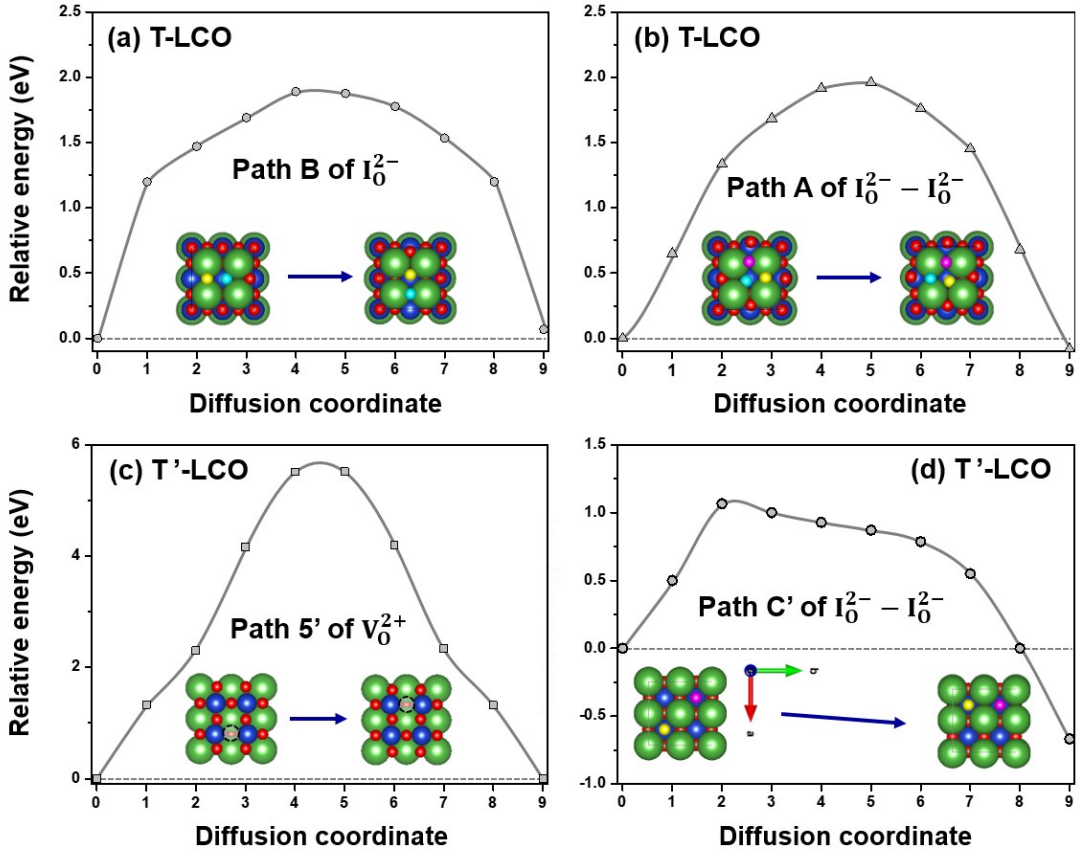

Figure S7. Energy landscapes obtained by climbing image-NEB calculations for **(a)** path B of I^{2-}_O in T-LCO, **(b)** path A of $I^{2-}_O - I^{2-}_O$ pair in T-LCO, **(c)** path 5' of V^{2+}_O in T'-LCO, and **(d)** path C' of $I^{2-}_O - I^{2-}_O$ pair in T'-LCO.

From experimental results of E_a = 0.81 eV for single crystalline T-LCO along the *c*-axis[16] and E_a = 1.18 eV for polycrystalline T-LCO[17], we can estimate that E_a for single crystalline T-LCO along the *ab*-plane should be higher than E_a= 1.18 eV for polycrystalline T-LCO, considering that polycrystalline phases usually have lower E_a for diffusion because of the presence of grain boundaries that offer fast diffusion pathways. Indeed, our experimental measurement and climbing image-NEB prediction results in the activation energy for oxygen diffusion of ~ 1.79 eV. Hence, we believe that our climbing image-NEB calculations are valid for the study of oxygen diffusion behavior in La_2CuO_4.

Moreover, in oxygen diffusion in T'-LCO (in Figure S7 (d)), the final configuration in the process is in a lower energy state than the initial configuration and this process can end up in oxygen trap in a

microscopic point of view. However, since both initial and final configurations can be generated without external potentials, as summarized in Figure 8 (b) in the main text, macroscopic oxygen diffusion in large specimens, after the diffusion process described in Figure S7 (d) occurs in the some microscopic areas simultaneously, similar configurations of the initial image can again be formed microscopically (also with recombination of one of interstitial pair and vacancies) and the diffusion process via the MEP (minimum energy path) shown in Figure S7(d). We belive this macroscopic diffusion process will actively occur via thermal excitation as in our experimental measurement at high temperatures (500 – 600 ℃).

References

1 A. Tsukada, M. Naito and H. Yamamoto, Valence of Ce in T- and T′-$La_{2-x}Ce_xCuO_4$, *Physica C: Superconductivity and its Applications*, 2007, **463–465**, 64–67.
2 M. Naito, A. Tsukada, T. Greibe and H. Sato, eds. I. Bozovic and D. Pavuna, Seattle, WA, 2002, p. 140.
3 S. Zhang and J. Northrup, Chemical potential dependence of defect formation energies in GaAs: Application to Ga self-diffusion, *Phys. Rev. Lett.*, 1991, **67**, 2339–2342.
4 N. Takahashi, T. Mizoguchi, T. Tohei, K. Nakamura, T. Nakagawa, N. Shibata, T. Yamamoto and Y. Ikuhara, First Principles Calculations of Vacancy Formation Energies in Σ13 Pyramidal Twin Grain Boundary of α-Al_2O_3, *Mater. Trans.*, 2009, **50**, 1019–1022.
5 C. Freysoldt, B. Grabowski, T. Hickel, J. Neugebauer, G. Kresse, A. Janotti and C. G. Van de Walle, First-principles calculations for point defects in solids, *Rev. Mod. Phys.*, 2014, **86**, 253–305.
6 A. Baldereschi, S. Baroni and R. Resta, Band Offsets in Lattice-Matched Heterojunctions: A Model and First-Principles Calculations for GaAs/AlAs, *Phys. Rev. Lett.*, 1988, **61**, 734–737.
7 K.-W. Park and C. S. Kim, Deformation-induced charge redistribution in ceria thin film at room temperature, *Acta Materialia*, 2020, **191**, 70–80.
8 T. Zacherle, A. Schriever, R. A. De Souza and M. Martin, *Ab initio* analysis of the defect structure of ceria, *Phys. Rev. B*, 2013, **87**, 134104.
9 W. Xie, Y.-L. Lee, Y. Shao-Horn and D. Morgan, Oxygen Point Defect Chemistry in Ruddlesden–Popper Oxides $(La_{1-x}Sr_x)_2MO_{4\pm\delta}$ (M = Co, Ni, Cu), *J. Phys. Chem. Lett.*, 2016, **7**, 1939–1944.
10 S. N. Savvin, G. N. Mazo and A. K. Ivanov-Schitz, Simulation of ion transport in layered cuprates $La_{2-x}Sr_xCuO_{4-\delta}$, *Crystallogr. Rep.*, 2008, **53**, 291–301.
11 E. J. Opila, G. Pfundtner, J. Maier, H. L. Tuller and B. J. Wuensch, Defect chemistry and transport properties in $YBa_2Cu_3O_{6+x}$ and (La, Sr)$_2CuO_4$*, *Materials Science and Engineering: B*, 1992, **13**, 165–168.
12 M.-Y. Su, E. A. Cooper, C. E. Elsbernd and T. O. Mason, High-Temperature Defect Structure of Lanthanum Cuprate, *J American Ceramic Society*, 1990, **73**, 3453–3456.
13 D. J. L. Hong and D. M. Smyth, Defect chemistry of undoped La_2CuO_4, *Journal of Solid State Chemistry*, 1992, **97**, 427–433.
14 H. Kanai, J. Mizusaki, H. Tagawa, S. Hoshiyama, K. Hirano, K. Fujita, M. Tezuka and T. Hashimoto, Defect Chemistry of $La_{2-x}Sr_xCuO_{4-\delta}$: Oxygen Nonstoichiometry and Thermodynamic Stability, *Journal of Solid State Chemistry*, 1997, **131**, 150–159.
15 E. J. Opila and H. L. Tuller, Thermogravimetric Analysis and Defect Models of the Oxygen Nonstoichiometry in $La_{2-x}Sr_xCuO_{4-y}$, *J American Ceramic Society*, 1994, **77**, 2727–2737.
16 E. J. Opila, H. L. Tuller, B. J. Wuensch and J. Maier, Oxygen Tracer Diffusion in $La_{2-x}Sr_xCuO_{4-y}$ Single Crystals, *J American Ceramic Society*, 1993, **76**, 2363–2369.

17 E. Boehm, J.-M. Bassat, M. C. Steil, P. Dordor, F. Mauvy and J.-C. Grenier, Oxygen transport properties of $La_2Ni_{1-x}Cu_xO_{4+\delta}$ mixed conducting oxides, *Solid State Sciences*, 2003, **5**, 973–981.